Research Square

Preprints are preliminary reports that have not undergone peer review.
They should not be considered conclusive, used to inform clinical practice,
or referenced by the media as validated information.

An electrochemical sensor based on ZnWO4/γ-Fe2O3 for detecting chloramphenicol in milk

Xiaodong Tu
Sichuan Provincial Institute of Science and Technology Talent
Mingcai Yao
Sichuan University of Science & Engineering
Liang Dong
dongliang@suse.edu.cn

Sichuan University of Science & Engineering

Research Article

Keywords: Electrochemical sensor, ZnWO4/γ-Fe2O3, Food analysis, Chloramphenicol

Posted Date: June 11th, 2026

DOI: https://doi.org/10.21203/rs.3.rs-9888012/v1

License: This work is licensed under a Creative Commons Attribution 4.0 International License.
Read Full License

Additional Declarations: Competing interest reported. The authors declare the following financial interests/personal relationships, which may be considered as potential competing interests: Liang Dong reports that financial support was provided by the Liquor Making Biological Technology & Application of Key Laboratory of Sichuan Province. Liang Dong reports that financial support was provided by the Postgraduate Education and Teaching Reform Project in Sichuan Province. Liang Dong reports that financial support was provided by the Teaching Reform Project of Sichuan University of Science & Engineering. Liang Dong reports that financial support was provided by the Postgraduate Teaching Construction Project of Sichuan University of Science & Engineering. Liang Dong reports that financial support was provided by the Postgraduate Quality Education and Teaching Resources Construction Project in Sichuan Province. If there are other authors, they declare that they have no known competing financial interests or personal relationships that could have appeared to influence the work reported in this paper.

Abstract

A chloramphenicol (CAP) electrochemical sensor based on zinc tungstate and magnetic hematite nanocomposites ($ZnWO_4$/γ-Fe_2O_3) is proposed. First, $ZnWO_4$ and γ-Fe_2O_3 nanomaterials were synthesized using a one-step hydrothermal method, then compositely modified onto glassy carbon electrodes to construct electrochemical sensors for measuring CAP. Under optimal conditions, the $ZnWO_4$/γ-Fe_2O_3-modified electrode exhibits a stronger reduction peak current for CAP detection than the single-component electrode and demonstrates better electrocatalytic activity. Results show that $ZnWO_4$/γ-Fe_2O_3/GCE has a linear range of 8-1000 μM and a detection limit of 1.04 μM, demonstrating good selectivity in the presence of different interferers, as well as outstanding stability and reproducibility. $ZnWO_4$/γ-Fe_2O_3/GCE was used for the detection of CAP in milk samples, yielding satisfactory results.

1. Instruction

Chloramphenicol (CAP) is a broad-spectrum antibiotic extracted from Streptomyces Venezuela, and gram-positive bacteria have a strong inhibitory effect on gram-negative bacteria. CAP was first isolated in 1947 because it significantly inhibits and destroys protein synthesis, is low-cost and high efficiency, and is widely used in the prevention and treatment of various infectious diseases in humans and animals(Z. Li et al., 2018; Wu et al., 2023). However, it was soon found that a small number of patients had aplastic anemia after using CAP, and it could be enriched between organisms, and the enrichment of CAP residues in animal foods would also have toxic effects on the human body(G. Gao et al., 2017). So the European Union, the United States, China, Japan, and other countries banned the use of CAP for food animals in the 80s and 90s of the 20th century(Chen et al., 2013). Despite this, it is still illegally used in animal husbandry due to its good antibacterial properties and low cost, and is still legally used in countries such as Brazil(Lofrano et al., 2016). Therefore, it is important to develop sensitive and rapid methods to monitor CAP residues in food.

For a long time, the detection of CAP mainly relies on gas chromatography (GC)(P. Li et al., 2006), high-performance liquid chromatography (HPLC)(Song et al., 2018), gas chromatography and mass spectrometry (GC-MS)(Samanidou et al., 2016), high-performance liquid chromatography and mass spectrometry (LC-MS)(Mao et al., 2021), enzyme-linked immunoassay(Wang et al., 2021), microbial detection(Zhao et al., 2022), fluorescence spectrophotometry(Manjula et al., 2021), these methods can meet the detection requirements, can be multi-component simultaneous analysis, but the equipment is expensive, the operation is cumbersome and time-consuming, and skilled technicians are required. The high demands placed on sample preparation, experimental environment, and operating conditions are limited in practical applications. In contrast, electrochemical sensor detection technology is a popular detection method with simple operation, low cost, fast response time, good sensitivity, repeatability, and accuracy(Z. Li et al., 2018; Ma et al., 2021).

The selection of highly electrocatalytically active materials to modify the electrode to improve sensitivity and stability has been a major challenge for CAP electrochemical detection(Qi et al., 2023). Metal oxide

nanomaterials have been widely studied in many fields and have been used in electrochemical detection, solar cells, supercapacitors, and photocatalysis. Recently, based on the advantages of numerous oxidation states, robust structural stability, high conductivity, and significant catalytic activity, multi-metal oxides have attracted great interest in various applications (Ding et al., 2021; dos Santos et al., 2021; Salah et al., 2018). In particular, binary transition metal oxides exhibit significant physicochemical properties and occupy a potential branch in the field of sensing(George et al., 2018). Recent trends in the use of this material in electrochemical research indicate that it has trace detection, simple preparation, rapid kinetics, easy operating conditions, highest selectivity, and sensitivity(Vinothkumar et al., 2021). Among them, zinc tungstate nanomaterials belong to rare earth nanostructured metal oxides in the huge oxide category, and their remarkable properties have attracted people's attention, and have been used in humidity sensors, optical fibers, catalysts, microwaves, microwaves, and photovoltaic electrochemical cells (Chung et al., 2017; Dhand et al., 2015; Ungelenk et al., 2014). Zinc tungstate has an increased electrical conductivity due to the presence of a W atom, and it also has a monoclinic wolframite structure with a band gap of 3.2 eV (Shad et al., 2019). Due to its high charge transfer ability, chemical stability, and catalytic activity (Phuruangrat et al., 2016), $ZnWO_4$ is a good material for modifying electrodes.

Iron oxide nanoparticles in magnetic materials, which have received great attention due to their significant activity in redox reactions and the detection of specific compounds such as hormones and viral particles (Molodtsova et al., 2022), have been explored for use in various fields, such as catalysis, magnetic materials, lithium-ion batteries, gas sensors, biosensing, and medical applications (Van Minh Hai et al., 2022). Fe_2O_3 is a typical n-type semiconductor with a narrow bandgap (2.2 eV) (Mo et al., 2021). To date, four Fe_2O_3 crystal forms that are easy to control by heat treatment have been reported: α-Fe_2O_3, β-Fe_2O_3, γ-Fe_2O_3, and ε-Fe_2O_3 (Tian et al., 2023). γ-Fe_2O_3 is one of the promising magnetic materials, which has a wide range of applications in high-density magnetic materials, catalysts, water treatment, pigments, and other applications (Zou et al., 2020). At the same time, γ-Fe_2O_3 has the advantages of low cost, conductivity, low toxicity, high sensitivity, relatively high saturation magnetization, and simple synthesis method, and can be converted to hematite phase (α-Fe_2O_3) at very high temperatures compared with Fe_3O_4 (Alotaibi et al., 2022; Mirzajani et al., 2018; Qin et al., 2023). To overcome the shortcomings of γ-Fe_2O_3-based sensors, which require high operating temperatures and exhibit poor selectivity, synthetic composites, controlled topography, and doping of precious metals are considered to be three effective methods for better practical applications (C. Zhang et al., 2020). Therefore, γ-Fe_2O_3 can be used as a good magnetic nanoparticle to replace Fe_3O_4 and further apply it to prepare composites.

In this paper, $ZnWO_4$/γ-Fe_2O_3 composite nanomaterials were prepared. Firstly, $ZnWO_4$ and γ-Fe_2O_3 nanomaterials were synthesized through a one-step hydrothermal method. Subsequently, these materials were combined and coated onto glassy carbon electrodes in the form of droplets. The results indicate that the $ZnWO_4$/γ-Fe_2O_3/GCE exhibits higher electrocatalytic activity compared to either

component alone when used for the detection of chloramphenicol residues. To our knowledge, this is the first time such a composite material has been used for the determination of chloramphenicol.

2. Materials and Methods

Reagent

Zinc acetate dihydrate ($Zn(CH_3COO)_2·2H_2O$, 99.99%), absolute ethanol (C_2H_5OH, 99.5%), glycerol ($C_3H_8O_3$, AR, 99%), sodium hydroxide (NaOH, AR, 96%), potassium ferrocyanide ($K_4[Fe(CN)_6]$, 98%), uric acid (99%), florfenicol (98%), and p-nitrophenol (AR), were purchased from Shanghai Macklin Biochemical Technology Co., Ltd. Ammonia (NH_3, AR, 25–28%), Sodium tungstate dihydrate ($Na_2WO_4·2H_2O$, 99.5%), ferric nitrate nonahydrate ($Fe(NO_3)_3·9H_2O$, AR), methanol (CH_3OH, AR, 99.5%), potassium chloride (KCl, AR), isopropanol (C_3H_8O, AR, 99.7%), clindamycin (≥ 99%), thiamphenicol (99%), and p-chlorophenol (AR, 99%), were purchased from Shanghai Aladdin Biochemical Technology Co., Ltd. Potassium ferricyanide ($K_3[Fe(CN)_6]$, AR), purchased from Shanghai Haohong Biomedical Technology Co., Ltd. Chloramphenicol (CAP, > 98.5%), was purchased from Guangzhou Saiguo Biotechnology Co., Ltd. Sodium chloride (NaCl, AR, 99.5%), phosphate buffer solution (0.01 M PBS, BR), and pH regulation using HCl and NaOH, were purchased from Shanghai Yuanye Biotechnology Co., Ltd. Hydrogen chloride (HCl, AR), was purchased from Chengdu Kelong Chemical Co., Ltd. Potassium nitrate (KNO_3, AR), was purchased from Chengdu Jinshan Chemical Reagent Co., Ltd.

Techniques

Using X-ray diffraction (XRD), purchased from Bruker D8 Advance, Germany; Analysis using Fourier transform infrared spectroscopy, purchased from Thermo Nicolet iS5; Using a scanning electron microscope (energy spectrum: Oxford ultim max 65), purchased from Tescan Mira4; Analysis of hysteresis loops using a vibrating sample magnetometer Model 7404, purchased from Lake Shore, USA; Electrochemical experiments were performed using CHI660E by cyclic voltammetry (CV) and differential pulse voltammetry (DPV) techniques. The three-electrode system is a saturated Ag/AgCl reference electrode, a glassy carbon electrode (GCE) working electrode, and a platinum (Pt) wire-to-pair electrode.

Synthesis of $ZnWO_4$ NP

The synthesis of $ZnWO_4$ NP was prepared by improving the typical synthesis method(Shad et al., 2019) by gradually adding 5 mM (20 mL) of sodium tungstate dihydrate [$Na_2WO_4·2H_2O$] to 15 mM (20 mL) of zinc acetate dihydrate [$Zn(CH_3COO)_2·2H_2O$] to form a milky white suspension, and then stirred for 1 h to ensure thorough mixing. Next, the pH of the mixed solution is adjusted to 10 by adding NaOH solution, and then hydrothermal treatment at 180 ℃ for 24 h in a stainless steel autoclave lined with PTFE. The resulting white precipitate is then washed 3 times with deionized water and ethanol to remove surface-bound contaminants. Dry the final product at 80 ℃ for 8 h and store it in a drying flask.

Preparation of γ-Fe $_2$ O $_3$

γ-Fe_2O_3 NP was prepared by typical synthesis methods(Qin et al., 2023). 0.271 g $Fe(NO_3)_3 \cdot 9H_2O$ was dissolved in a mixed solution of 10 mL glycerol and 70 mL of isopropanol, magnetically stirred for 10 min, and then the uniformly clear solution was poured into a 100 mL Teflon-lined stainless steel autoclave and reacted at 190 ℃ for 12 h. After cooling the autoclave to room temperature, centrifuge the product and wash it 3 times with deionized water and ethanol, then dry at 70 ℃ for 12 h. The product was then placed in a tube furnace and calcined at 350 ℃ for 2 h in an N_2 and air atmosphere at a heating rate of 1 ℃ min^{-1}, respectively, to obtain reddish-brown powder, which was stored in a drying flask.

Synthesis of ZnWO $_4$ /γ-Fe $_2$ O $_3$ nanocomposites

The preparation of $ZnWO_4$/γ-Fe_2O_3 was based on the synthesis method of Malik(Malik et al., 2023), and some improvements were made. The method is as follows: to introduce γ-Fe_2O_3 on the surface of the prepared $ZnWO_4$, 40 mg of $ZnWO_4$ was dispersed in a solution containing 4 mL of ethanol and 400 µL of NH_3 (25%). Then, add 20 mg of γ-Fe_2O_3 to the solution and sonicate the mixture for 2 h. Finally, $ZnWO_4$/γ-Fe_2O_3 is magnetically separated, washed 3 times with ethanol, and dried at 80 ℃ for 10 h, storing it in a drying flask.

Preparation of ZnWO $_4$ /γ-Fe $_2$ O $_3$ /GCE electrodes

Prior to each electrochemical measurement, the electrodes were modified following the method described by Vinothkumar(Vinothkumar et al., 2021). The electrodes were polished for 3 minutes on a smooth polishing cloth using 1.5 µm alumina, then cleaned with anhydrous ethanol and distilled water before being dried. Subsequently, 5 mg of the $ZnWO_4$/γ-Fe_2O_3 nanocomposite was mixed with 1 ml of anhydrous ethanol and ultrasonicated for 20 minutes. After that, 6 µL of the resulting solution was applied onto the surface of a glassy carbon electrode (GCE) and dried in an oven at 60 ℃ for 10 minutes. The prepared electrodes were then used to measure the concentration of chloramphenicol using CV and DPV techniques according to standard procedures. The experimental setup is illustrated in Fig. 1.

Electrochemical measurements

To assess the CV and DPV behavior of chloramphenicol, 10 mL of 0.01 M PBS (pH 7.4) was injected into the measurement cell; Then, a solution of chloramphenicol in different concentration ranges was injected into it with a micropipette. $ZnWO_4$/γ-Fe_2O_3/GCE was placed in the measurement cell, and the prepared solution was vigorously stirred for 10 min. After that, the agitation was stopped, and electrochemical measurements were performed by CV and DPV at room temperature. The electrochemical workstation of the three-electrode system was used for electrochemical measurement,

with the glass-carbon electrode as the working electrode, the platinum wire as the counter-electrode, and Ag/AgCl as the reference electrode.

Actual sample testing

Electrochemical testing of milk in actual samples was conducted using methods by Sakaleshpur Kumar(Sakaleshpur Kumar et al., 2024), with pretreatment followed by subsequent experiments. Milk samples were purchased from school supermarkets and diluted in PBS buffer with pH = 7.4. The mixture was then centrifuged at 6000 rpm/min for 10 minutes. After centrifugation, the supernatant was separated and stored at 4 ℃. CAP was added to milk samples at specified concentrations (10, 20, 30, 40, and 50 μM) using standard addition methods, and DPV current responses were recorded.

3 Results and Discussion

Structural Analysis of $ZnWO_4$/γ-Fe_2O_3 Nanocomposites

The morphology of the synthesized materials was studied using a scanning electron microscope (SEM). As shown in Fig. 2a, $ZnWO_4$ exhibits spherical structures of various sizes; some of these particles aggregate into irregular flaky formations, and it can be observed that these flaky layers are closely stacked on top of each other. The SEM image of the $ZnWO_4$/γ-Fe_2O_3 composite material (Fig. 2b) reveals that $ZnWO_4$ is dispersed among the flaky γ-Fe_2O_3 particles, with some $ZnWO_4$ particles adhering to the surface of γ-Fe_2O_3. This arrangement makes the spherical shape of $ZnWO_4$ more distinct and also increases the contact area between the composite material and the analytes, thereby enhancing the catalytic properties of the material. In addition, element analysis using EDS and mapping techniques was conducted to identify the constituent elements (Zn, W, Fe, and O). The contents of these elements were determined to be 26.86%, 24.35%, 12.13%, and 36.66%, respectively. These results confirm that the mass ratio parameters used in the MMIP preparation method (a mass ratio of 1:2 for γ-Fe_2O_3 to $ZnWO_4$) were appropriate, indicating the successful formation of the $ZnWO_4$/γ-Fe_2O_3 composite material (Fig. 2c). Figure 2d-h confirms the uniform diffusion of Zn, W, Fe, and O elements within the $ZnWO_4$/γ-Fe_2O_3 composite material. The high specific surface area, favorable surface morphology, and uniform chemical composition (as determined by EDS and mapping analyses) demonstrate that the proposed $ZnWO_4$/γ-Fe_2O_3 composite material is capable of further enhancing its excellent electrochemical properties(George et al., 2018).

The crystalline phase and purity of the $ZnWO_4$/γ-Fe_2O_3 composite material were analyzed using XRD of the powder samples, as shown in Fig. 3a. The diffraction patterns of the $ZnWO_4$ nanoparticles resembled those of the standard JCPDS structure of pure $ZnWO_4$ (No. 15–0774), indicating the formation of monoclinic $ZnWO_4$ nanoparticles(Sun et al., 2022). In the XRD spectra of the $ZnWO_4$/γ-Fe_2O_3 composite material, typical peaks characteristic of γ-Fe_2O_3 nanoparticles were observed at 2θ = 18.5°, 22.4°, 30.3°, 35.7°, 38.3°, 40.1°, 43.3°, and 62.8°, confirming the successful preparation of the

composite material(Tian et al., 2023). Infrared spectroscopy (FT-IR) was performed in the wavelength range of 400 to 4000 cm^{-1} on $ZnWO_4$, γ-Fe_2O_3, and the $ZnWO_4$/γ-Fe_2O_3 composite materials, as shown in Fig. 3b. For the $ZnWO_4$ nanoparticles, infrared peaks at 466.75 cm^{-1}, 832.90 cm^{-1}, 1394.52 cm^{-1}, and 1507.59 cm^{-1} were attributed to the bending and stretching movements of Zn-O-W bonds(Sun et al., 2022). In γ-Fe_2O_3 nanoparticles, the spectra at 560.06 cm^{-1} and 637.87 cm^{-1} exhibit two prominent double peaks associated with the Fe-O bonds(Kuzharov et al., 2022). The Fourier transform infrared spectra of the $ZnWO_4$/γ-Fe_2O_3 composite materials reveal the bending and stretching vibrations of both the Zn-O-W bonds and the Fe-O bonds. The results indicate that the synthesized $ZnWO_4$/γ-Fe_2O_3 mixture indeed consists of $ZnWO_4$ and γ-Fe_2O_3, in accordance with the findings obtained from XRD analysis. Since all three materials were synthesized in aqueous solutions, the broad peak in the range of 3300–3500 cm^{-1} observed in all spectra is attributed to the O-H stretching vibrations on the surface of the materials, which are absorbed by water(Kuzharov et al., 2022).

The magnetism of γ-Fe_2O_3 and $ZnWO_4$/γ-Fe_2O_3 was studied using a vibrating sample magnetometer. As shown in Fig. 3c, at room temperature, the coercivity or residuality of γ-Fe_2O_3 and $ZnWO_4$/γ-Fe_2O_3 is almost zero, indicating that both possess superparamagnetic properties. The saturation magnetization strengths of γ-Fe_2O_3 and $ZnWO_4$/γ-Fe_2O_3 were 46.17 (emu/g) and 26.56 (emu/g), respectively. It can be seen that the addition of $ZnWO_4$ weakens the magnetic strength of $ZnWO_4$/γ-Fe_2O_3 composites, which also confirms the characterization results from SEM, XRD, and FTIR. Therefore, the magnetism of $ZnWO_4$/γ-Fe_2O_3 composites can be used to separate them from the solution under the conditions of an applied magnetic field.

Optimization of experimental conditions

The experimental conditions were optimized for the electrocatalytic activity of 250 μM CAP in 0.01 M PBS (pH = 7.4) solution, except for the cyclic voltammetry (CV) method for the pH optimization of phosphate buffer solution, and the results were obtained by differential pulsed voltammetry (DPV). In order to determine the addition of γ-Fe_2O_3 and $ZnWO_4$ in the composites, the electrocatalytic activities of γ-Fe_2O_3 and $ZnWO_4$ at different addition mass ratios of 1:1, 1:2, 1:3, 1:4, 1:5 and 1:6 were investigated. As shown in Fig. 4a, the addition of a mass ratio of 1:2 is the largest current difference ΔI, while with the addition of zinc tungstate mass, the current difference decreases, and when the mass ratio is increased to 1:4, ΔI tends to stabilize. Therefore, we chose a 1:2 mass ratio of γ-Fe_2O_3 and $ZnWO_4$ as the optimal addition amount for the electrochemical experiment.

The effect of pH on the DPV current response of 250 μM CAP on $ZnWO_4$/γ-Fe_2O_3/GCE was observed in PBS (0.01 M) solution under various pH values ranging from 3.0 to 11.0, as shown in Fig. 4b. At the same time, since the normal human pH is between 7.35 ~ 7.45, pH 7.4 was also selected for optimization. As shown in the figure, when pH increases from 3.0 to 7.4, the peak reduction current increases rapidly. After pH increases from 9.0 to 11.0, the reducing current drops rapidly. Therefore, considering higher

sensitivity, the maximum reducing current is reached at pH 7.4, and this buffer solution can be used for further electrochemical methods(Vinothkumar et al., 2021).

Before conducting the current analysis and measurement, the electrocatalytic activity of $ZnWO_4$/γ-Fe_2O_3 under different loads of 2, 4, 6, 8, and 10 µL was investigated. As shown in Fig. 4c, within a load range of 2 ~ 6 µL, the reduction current difference ΔI on the prepared electrode increases rapidly with the load, and when the load exceeds 6.0 µL, the current difference ΔI decreases significantly. Therefore, we selected 6.0 µL of $ZnWO_4$/γ-Fe_2O_3 solution as the optimal loading capacity for the electrochemical experiment.

Electrochemical characterization of $ZnWO_4$/γ-Fe_2O_3

Electrochemical impedance spectra (EIS) of GCE, $ZnWO_4$/GCE, γ-Fe_2O_3/GCE, and $ZnWO_4$/γ-Fe_2O_3/GCE were studied in 0.1 M KCl and 5.0 mM $[Fe(CN)_6]^{3-/4-}$ solution, with a recognition voltage of 5 mV and a frequency range of 100 kHz to 0.01 Hz, as shown in Fig. 5a. In a typical Nyquist curve, the high-frequency region appears as a semicircle, the low-frequency region is monitored by a linear region, and the diameter of the semicircle is Rct. Impedance maps were fitted using ZSimpWin software, yielding R_{ct} values for GCE, $ZnWO_4$/GCE, γ-Fe_2O_3/GCE, and $ZnWO_4$/γ-Fe_2O_3/GCE for Nyquist plots of 472.7 Ω, 38680 Ω, 4869 Ω, and 19840 Ω, respectively. It can be observed that GCE electrodes have the lowest resistance, and γ-Fe_2O_3/GCE exhibits very low impedance. After combining γ-Fe_2O_3 and $ZnWO_4$ NP, the impedance is significantly reduced compared to $ZnWO_4$. These results indicate that the introduction of γ-Fe_2O_3 nanomaterials improves the conductivity of $ZnWO_4$ NP, further confirming the original intention of modified $ZnWO_4$, which can promote electron transfer at the electrode interface. The synergistic effect of $ZnWO_4$ and γ-Fe_2O_3 can enhance the electrocatalytic performance of the composite material and also confirm the successful synthesis of $ZnWO_4$/γ-Fe_2O_3 composites. The CV curves of the modified electrodes were studied in 0.1 M KCl and 5 mM $[Fe(CN)_6]^{3-/4-}$ solution (Fig. 5b), and the results matched the electrochemical impedance spectrum. The bare GCE had the highest redox current, while due to the high impedance of $ZnWO_4$/GCE, its redox current was the lowest. After the introduction of γ-Fe_2O_3 nanomaterials, the electrocatalytic performance of $ZnWO_4$ was significantly improved, greatly increasing its peak redox current.

Figure 5c investigates the CV curves of different modified electrodes containing 250 µM CAP in 0.01 mM PBS solution, and in the absence of CAP, the proposed electrodes have no peak response, respectively. As can be seen from the figure, the bare GCE exhibits a significant reduction peak response at I_{pc} = -10.97 µA, with a reduction peak potential of -0.72 V. After the modified $ZnWO_4$/GCE, the peak current increased slightly (I_{pc} = -12 µA) and the reduction peak potential was − 0.71 V. After the addition of γ-Fe_2O_3, the peak current of the $ZnWO_4$/γ-Fe_2O_3 composite modified electrode was significantly increased (I_{pc}=-18.15 µA), and the reduction peak potential was − 0.75 V. The increase in current may be due to the significant activity and electrocatalytic properties of γ-Fe_2O_3, which increases the contact area between

the composite and the CAP, and its synergistic interaction with $ZnWO_4$ makes it exhibit a strong current response(Molodtsova et al., 2022).

Sensor electrochemical measurement

Under optimal conditions, the electrochemical response of $ZnWO_4$/γ-Fe_2O_3/GCE at different concentrations of CAP in 0.01M PBS solution (pH = 7.4) was determined by differential pulsed voltammetry (DPV). As can be seen from Fig. 6a, from 8 ~ 1000 μM, the reduction peak current increases with increasing CAP concentration. The linear plot of the reduction current to CAP concentration is shown in Fig. 6b, and the linear regression equation is: I_{pc} (μA) = 0.01061C [μM] + 0.07883 (R^2 = 0.9934). The LOD and LOQ of the CAP are calculated using the following formulas (1) and (2) (Forootan et al., 2017):

$$LOD = \frac{3\sigma}{k}$$

1

$$LOQ = \frac{10\sigma}{k}$$

2

where σ is the standard deviation calculated from the values of 10 blank samples, and k is the slope of the linear regression. The LOD and LOQ were calculated to be 1.04 μM and 3.47 μM, with a sensitivity of 0.1501 μA μM^{-1} cm^{-2}. In addition, Table 1 compares the detection performance of the sensors prepared in this chapter with the different previously proposed sensors by modifying the electrodes, detection techniques, linear ranges, and detection limits. From the results of Table 1, it can be seen that the electrodes prepared in this study have a wide linear range and a low detection limit, and $ZnWO_4$/γ-Fe_2O_3/GCE has higher adsorption capacity, detection efficiency, and excellent electroreduction activity compared with other electrochemical sensors.

Table 1
Performance comparison of $ZnWO_4$/γ-Fe_2O_3/GCE with other modified electrodes

Electrode	Method	Linear range (μM)	Detection limit (μM)	Ref.
$ZnWO_4$/GCE	CV	30–500	0.32	(Shad et al., 2019)
Fe_3O_4/GCE	SWV	0.09-47	0.09	(Giribabu et al., 2017)
MoS_2-rGO/GCE	DPV	5–35	1	(S. Gao et al., 2021)
rGO/PDA/AuNPs/GCE	DPV	0.1–100	0.058	(L. Zhang et al., 2022)
$ZnWO_4$/γ-Fe_2O_3/GCE	DPV	8-1000	1.04	This work
PDA = polydopamine				

Sensor selectivity, repeatability, and stability

For the further practical application of CAP detection, selectivity, repeatability, and stability are of paramount importance. Figure 7a shows the relative error in CAP detection using a $ZnWO_4$/γ-Fe_2O_3/GCE electrode in a solution containing 0.01M PBS (pH = 7.4) in the presence of interfering substances. As illustrated, during the detection of 10 μM CAP, interferents such as thiamphenicol (TH), clindamycin (CL), 4-chlorophenol (4-CP), 4-nitrophenol (4-NP), uric acid (UA), glucose (Glu), sodium chloride (NaCl), and potassium nitrate (KNO_3) (Vinothkumar et al., 2021) caused only minor changes in current, with the current signals remaining below 8%. This indicates that the $ZnWO_4$/γ-Fe_2O_3/GCE electrode exhibits good selectivity for CAP detection.

The current responses of five different GCEs modified with $ZnWO_4$/γ-Fe_2O_3 to CAP were simultaneously measured in order to evaluate the repeatability of the electrodes. As shown in Fig. 7b, the calculated relative standard deviation (RSD) was 1.03%, indicating that the $ZnWO_4$/γ-Fe_2O_3/MIP/GCEs exhibit good reproducibility. In addition, the long-term stability of the $ZnWO_4$/γ-Fe_2O_3/MIP/GCEs in detecting CAP was tested over a period of 28 days using a single modified electrode. Figure 7c shows that the electrode current decreased by less than 15% within these 28 days, confirming the excellent stability of the modified electrodes.

Determination of actual samples

To evaluate the suitability of $ZnWO_4$/γ-Fe_2O_3/GCE, milk was pretreated, and subsequent experiments were performed. Figure 7d shows the DPV curve of the milk sample with CAP added. As shown in Table 2, we compared the CAP parameters in food samples detected by Sakaleshpur Kumar et al. using liquid chromatography-mass spectrometry (LC-MS) techniques during the analysis. The experimental results showed that there was no significant difference between the two methods, and the recovery rate

of the spiked samples was between 96.3 ~ 98.9%, and the RSD was less than 3.42%. The results of this study show that $ZnWO_4$/γ-Fe_2O_3/GCE shows acceptable recovery in detecting CAP in milk samples, making it a suitable platform for real-time analysis of milk samples.

Table 2
Determination of CAP in milk using the $ZnWO_4$/γ-Fe_2O_3/GCE sensor

Samples	Added (μM)	Found (μM)		Recovery (%)		RSD (%)	
		DPV	LC-MS	DPV	LC-MS	DPV	LC-MS
1	10	9.73	9.82	97.3	98.2	2.65	1.96
2	20	19.26	18.45	96.3	92.2	2.18	2.88
3	30	29.68	29.11	98.9	97.0	2.85	2.03
4	40	39.19	39.21	98.0	98.0	1.68	2.11
5	50	49.28	49.35	98.6	98.7	3.42	1.98

4. Conclusion

$ZnWO_4$ and γ-Fe_2O_3 basic nanomaterials were synthesized by a one-step hydrothermal method, and $ZnWO_4$/γ-Fe_2O_3 nanomaterials were compositely prepared, and $ZnWO_4$/γ-Fe_2O_3/GCE sensors were constructed for CAP detection. The results showed that it exhibited superior selectivity, stability, and electrocatalytic performance than $ZnWO_4$, with a wide linear range (8 ~ 1000 μM) and a LOD as low as 1.04 μM (S/N = 3). The recoveries of this sensor for CAP detection in milk are between 96.3 ~ 98.9% (RSD < 3.42%), with good reproducibility and low interference, providing a practical sensing platform for the detection of chloramphenicol in milk. At the same time, this study provides an effective strategy for the selection and application of magnetic materials to replace Fe_3O_4.

Declarations

Declaration of Competing Interest

The authors declare the following financial interests/personal relationships, which may be considered as potential competing interests:

Competing Interests

The authors declare the following financial interests/personal relationships, which may be considered as potential competing interests:Liang Dong reports that financial support was provided by the Liquor Making Biological Technology & Application of Key Laboratory of Sichuan Province. Liang Dong reports that financial support was provided by the Postgraduate Education and Teaching Reform Project in

Sichuan Province. Liang Dong reports that financial support was provided by the Teaching Reform Project of Sichuan University of Science & Engineering. Liang Dong reports that financial support was provided by the Postgraduate Teaching Construction Project of Sichuan University of Science & Engineering. Liang Dong reports that financial support was provided by the Postgraduate Quality Education and Teaching Resources Construction Project in Sichuan Province. If there are other authors, they declare that they have no known competing financial interests or personal relationships that could have appeared to influence the work reported in this paper.

Funding:

This work was supported by the Liquor Making Biological Technology & Application of Key Laboratory of Sichuan Province [grant number NJ2021-05]; Postgraduate Quality Education and Teaching Resources Construction Project in Sichuan Province; Postgraduate Education and Teaching Reform Project in Sichuan Province [grant number YJGXM24-C045]; Teaching Reform Project of Sichuan University of Science & Engineering [grant number JG-2359]; and Postgraduate Teaching Construction Project of Sichuan University of Science & Engineering [grant number AL202309].

Author Contribution

Tu, X: Conceptualization, Methodology, Data curation, Visualization, Writing - original draft. Yao, M: Conceptualization, Supervision, Writing - review & editing. Dong, L: Conceptualization, Funding acquisition, Project administration, Supervision, Writing - review & editing. All authors reviewed the manuscript.

Data availability

Data will be made available on request.

References

1. Alotaibi I, Alshammari MS, Algessair S, Madkhali N, All NA, Hjiri M, Alrub SA, El Mir L, Lemine OM (2022) Synthesis, characterization and heating efficiency of Gd-doped maghemite (γ-Fe_2O_3) nanoparticles for hyperthermia application. Phys B Condens Matter 625:413510. https://doi.org/10.1016/j.physb.2021.413510
2. Chen L, Li B (2013) Magnetic molecularly imprinted polymer extraction of chloramphenicol from honey. Food Chem 141(1):23–28. https://doi.org/10.1016/j.foodchem.2013.02.085
3. Chung DY, Jun SW, Yoon G, Kim H, Yoo JM, Lee K-S, Kim T, Shin H, Sinha AK, Kwon SG, Kang K, Hyeon T, Sung Y-E (2017) Large-Scale Synthesis of Carbon-Shell-Coated FeP Nanoparticles for

Robust Hydrogen Evolution Reaction Electrocatalyst. JACS 139(19):6669–6674. https://doi.org/10.1021/jacs.7b01530

4. Dhand C, Dwivedi N, Loh XJ, Jie Ying AN, Verma NK, Beuerman RW, Lakshminarayanan R, Ramakrishna S (2015) Methods and strategies for the synthesis of diverse nanoparticles and their applications: a comprehensive overview. RSC Adv 5(127):105003–105037. https://doi.org/10.1039/C5RA19388E
5. Ding C, Jia H, Sun Q, Yao Z, Yang H, Liu W, Pang X, Li S, Liu C, Minari T, Chen J, Liu X, Song Y (2021) Wafer-scale single crystals: crystal growth mechanisms, fabrication methods, and functional applications. J Mater Chem C Mater 9(25):7829–7851. https://doi.org/10.1039/D1TC01101D
6. dos Santos OAL, Sneha M, Devarani T, Bououdina M, Backx BP, Vijaya JJ, Bellucci S (2021) Review—Perovskite/Spinel Based Graphene Derivatives Electrochemical and Biosensors. J Electrochem Soc 168(6):067506. https://doi.org/10.1149/1945-7111/ac0306
7. Forootan A, Sjöback R, Björkman J, Sjögreen B, Linz L, Kubista M (2017) Methods to determine limit of detection and limit of quantification in quantitative real-time PCR (qPCR). Biomol Detect Quantif 12:1–6. https://doi.org/10.1016/j.bdq.2017.04.001
8. Gao G, Chen H, Liu P, Hao Z, Ma G, Chai Y, Wang C, Lu C (2017) Residue pattern of polycyclic aromatic hydrocarbons during green tea manufacturing and their transfer rates during tea brewing. Food Addit Contam Part Chem Anal Control Expo Risk Assess 34(6):990–999. https://doi.org/10.1080/19440049.2017.1316873
9. Gao S, Zhang Y, Yang Z, Fei T, Liu S, Zhang T (2021) Electrochemical chloramphenicol sensors-based on trace MoS_2 modified carbon nanomaterials: Insight into carbon supports. J Alloys Compd 872:159687. https://doi.org/10.1016/j.jallcom.2021.159687
10. George JM, Antony A, Mathew B (2018) Metal oxide nanoparticles in electrochemical sensing and biosensing: a review. Mikrochim Acta 185(7):358. https://doi.org/10.1007/s00604-018-2894-3
11. Giribabu K, Jang S-C, Haldorai Y, Rethinasabapathy M, Oh SY, Rengaraj A, Han YK, Cho W-S, Roh C, Huh YS (2017) Electrochemical determination of chloramphenicol using a glassy carbon electrode modified with dendrite-like Fe_3O_4 nanoparticles. Carbon Lett 23:38–47. https://doi.org/10.5714/CL.2017.23.038
12. Kuzharov AA, Gritsai MA, Butova VV, Soldatov MA, Polyakov VA, Rud PA, Rusalev YV, Kubrin SP, Roldugin VA, Trigub AL, Soldatov AV (2022) One-step electrochemical synthesis of γ-Fe_2O_3@MIL-88a magnetic composite for heterogeneous Fenton-like catalysis. Ceram Int 48(23, Part A): 34864–34876. https://doi.org/10.1016/j.ceramint.2022.08.076
13. Li P, Qiu Y, Cai H, Kong Y, Tang Y, Wang D, Xie M (2006) Simultaneous Determination of Chloramphenicol, Thiamphenicol, and Florfenicol Residues in Animal Tissues by Gas Chromatography/Mass Spectrometry. Se Pu 24(1):14–18. https://doi.org/10.1016/S1872-2059(06)60002-3
14. Li Z, Lei C, Wang N, Jiang X, Zeng Y, Fu Z, Zou L, He L, Liu S, Ao X, Zhou K, Chen S (2018) Preparation of magnetic molecularly imprinted polymers with double functional monomers for the extraction

and detection of chloramphenicol in food. J Chromatogr B 1100–1101:113–121. https://doi.org/10.1016/j.jchromb.2018.09.032

15. Lofrano G, Libralato G, Adinolfi R, Siciliano A, Iannece P, Guida M, Giugni M, Ghirardini V, A., Carotenuto M (2016) Photocatalytic degradation of the antibiotic chloramphenicol and effluent toxicity effects. Ecotoxicol Environ Saf 123:65–71. https://doi.org/10.1016/j.ecoenv.2015.07.039
16. Ma Y, Li J, Wang L (2021) Porous carbon derived from ZIF-8 modified molecularly imprinted electrochemical sensor for the detection of tert-butyl hydroquinone (TBHQ) in edible oil. Food Chem 365:130462. https://doi.org/10.1016/j.foodchem.2021.130462
17. Malik S, Khan A, Khan H, Rahman G, Ali N, Khan S, Sotomayor MDPT (2023) Biomimetic Electrochemical Sensors Based on Core-Shell Imprinted Polymers for Targeted Sunset Yellow Estimation in Environmental Samples. Biosensors 13(4):429. https://doi.org/10.3390/bios13040429
18. Manjula N, Chen S-M (2021) Synthesis of highly electroactive nanoflowers like manganesetin oxide and electroanalytical application for chloramphenicol determination in milk and honey samples. J Electroanal Chem 880:114914. https://doi.org/10.1016/j.jelechem.2020.114914
19. Mao N, Sun Z, Zhang L (2021) Determination of 6 Antibiotics Residues in Farm Soil by HPLC-MS/MS. Chem Reagents 43(7):945–950. https://doi:10.13822/j.cnki.hxsj.2021008015
20. Mirzajani R, Karimi S (2018) Preparation of γ-Fe_2O_3/hydroxyapatite/Cu(II) magnetic nanocomposite and its application for electrochemical detection of metformin in urine and pharmaceutical samples. Sens Actuators B Chem 270:405–416. https://doi.org/10.1016/j.snb.2018.05.032
21. Mo R, Han D, Yang C, Tang J, Wang F, Li C (2021) MOF-derived porous Fe_2O_3 nanocubes combined with reduced graphene oxide for n-butanol room temperature gas sensing. Sens Actuators B Chem 330:129326. https://doi.org/10.1016/j.snb.2020.129326
22. Molodtsova T, Gorshenkov M, Kubrin S, Saraev A, Ulyankina A, Smirnova N (2022) One-step access to bifunctional γ-Fe_2O_3/δ-FeOOH electrocatalyst for oxygen reduction reaction and acetaminophen sensing. J Taiwan Inst Chem Eng 140:104569. https://doi.org/10.1016/j.jtice.2022.104569
23. Phuruangrat A, Dumrongrojthanath P, Thongtem S, Thongtem T (2016) Influence of Dy dopant on photocatalytic properties of Dy-doped $ZnWO_4$ nanorods. Mater Lett 166:183–187. https://doi.org/10.1016/j.matlet.2015.12.071
24. Qi X, Teng Z, Yu J, Jia D, Zhang Y, Pan H (2023) A simple one-step synthesis of Fe_3O_4/N-rGO nanocomposite for sensitive electrochemical detection of chloramphenicol. Mater Lett 330:133350. https://doi.org/10.1016/j.matlet.2022.133350
25. Qin Q, Zhang X, Zhang N (2023) High response and excellent selectivity acetone sensor based on γ-Fe_2O_3 hollow microspheres. Mater Lett 330:133337. https://doi.org/10.1016/j.matlet.2022.133337
26. Sakaleshpur Kumar G, Ballur Prasanna S, Lokesh Marenahalli B, Shadakshari S, Arehalli Shivamurthy S, Rajabathar JR, Shanthakumar C, K., Han Y-K (2024) Flake-like structure of $SrTiO_3$ nanoparticles dispersed on graphene oxide: A selective and sensitive electrochemical sensor for determination of

chloramphenicol in milk and honey samples. Food Chem 444:138637. https://doi.org/10.1016/j.foodchem.2024.138637

27. Salah LM, Mabied AF, Abdellatif MH (2018) Multiferroic property of Ca1-xLaxTi1-xFexO_3 perovskite structure. J Magn Magn Mater 458:10–14. https://doi.org/10.1016/j.jmmm.2018.02.062
28. Samanidou V, Kehagia M, Kabir A, Furton KG (2016) Matrix molecularly imprinted mesoporous sol–gel sorbent for efficient solid-phase extraction of chloramphenicol from milk. Anal Chim Acta 914:62–74. https://doi.org/10.1016/j.aca.2016.02.003
29. Shad NA, Bajwa SZ, Amin N, Taj A, Hameed S, Khan Y, Dai Z, Cao C, Khan WS (2019) Solution growth of 1D zinc tungstate ($ZnWO_4$) nanowires; design, morphology, and electrochemical sensor fabrication for selective detection of chloramphenicol. J Hazard Mater 367:205–214. https://doi.org/10.1016/j.jhazmat.2018.12.072
30. Song X, Xie J, Zhang M, Zhang Y, Li J, Huang Q, He L (2018) Simultaneous determination of eight cyclopolypeptide antibiotics in feed by high performance liquid chromatography coupled with evaporation light scattering detection. J Chromatogr B 1076:103–109. https://doi.org/10.1016/j.jchromb.2018.01.020
31. Sun L, Hou C, Sun J, Mo Q, Han J, Bai S, Luo R (2022) One-step calcined equiatomic W and Zn precursors to synthesize heterojunction of ZnO/$ZnWO_4$ for NO_2 detection. Sens Actuators B Chem 367:131987. https://doi.org/10.1016/j.snb.2022.131987
32. Tian R, Gao Z, Chen G, Guan H, Dong C, Comini E (2023) Functionalized Pt nanoparticles between α/γ-Fe_2O_3 and MXene for superior acetone sensing. Sens Actuators B Chem 383:133584. https://doi.org/10.1016/j.snb.2023.133584
33. Ungelenk J, Speldrich M, Dronskowski R, Feldmann C (2014) Polyol-mediated low-temperature synthesis of crystalline tungstate nanoparticles MWO_4 (M = Mn, Fe, Co, Ni, Cu, Zn). Solid State Sci 31:62–69. https://doi.org/10.1016/j.solidstatesciences.2014.02.020
34. Van Hai M, Cuong H, Mai ND, Long HD, Phuong HT, Dang TQ, Thong TK, Viet LV, N. N., Van Hieu N (2022) Superior detection and classification of ethanol and acetone using 3D ultra-porous γ-Fe_2O_3 nanocubes-based sensor. Sens Actuators B Chem 362:131737. https://doi.org/10.1016/j.snb.2022.131737
35. Vinothkumar V, Abinaya M, Chen S-M (2021) Ultrasonic assisted preparation of $CoMoO_4$ nanoparticles modified electrochemical sensor for chloramphenicol determination. J Solid State Chem 302:122392. https://doi.org/10.1016/j.jssc.2021.122392
36. Wang X, Li J, Jian D, Zhang Y, Shan Y, Wang S, Liu F (2021) Paper-based antibiotic sensor (PAS) relying on colorimetric indirect competitive enzyme-linked immunosorbent assay for quantitative tetracycline and chloramphenicol detection. Sens Actuators B Chem 329:129173. https://doi.org/10.1016/j.snb.2020.129173
37. Wu X, Chen J, Yao R, Xie C (2023) Research Progress of Electrochemical Sensor Detection Technology for Chloramphenicol. Chem Reagents 45(03):85–93.

https://doi:10.13822/j.cnki.hxsj.2022.0832

38. Zhang C, Zhang S, Yang Y, Yu H, Dong X (2020) Highly sensitive H_2S sensors based on metal-organic framework driven γ-Fe_2O_3 on reduced graphene oxide composites at room temperature. Sens Actuators B Chem 325:128804. https://doi.org/10.1016/j.snb.2020.128804
39. Zhang L, Yin M, Wei X, Sun Y, Chen Y, Qi S, Tian X, Qiu J, Xu D (2022) Synthesis of rGO@PDA@AuNPs for an effective electrochemical chloramphenicol sensor. Diam Relat Mater 128:109311. https://doi.org/10.1016/j.diamond.2022.109311
40. Zhao Q, Liu X (2022) Study on the Rapid Detection Method of Antibiotic Residues in Animal-Derived Foods. Mod Food 28(02):75–77. https://doi:10.16736/j.cnki.cn41-1434/ts.2022.02.023
41. Zou C, Hu J, Su Y, Zhou Z, Cai B, Tao Z, Huo T, Hu N, Zhang Y (2020) Highly repeatable and sensitive three-dimensional γ-Fe_2O_3@reduced graphene oxide gas sensors by magnetic-field assisted assembly process. Sens Actuators B Chem 306:127546. https://doi.org/10.1016/j.snb.2019.127546

Figures

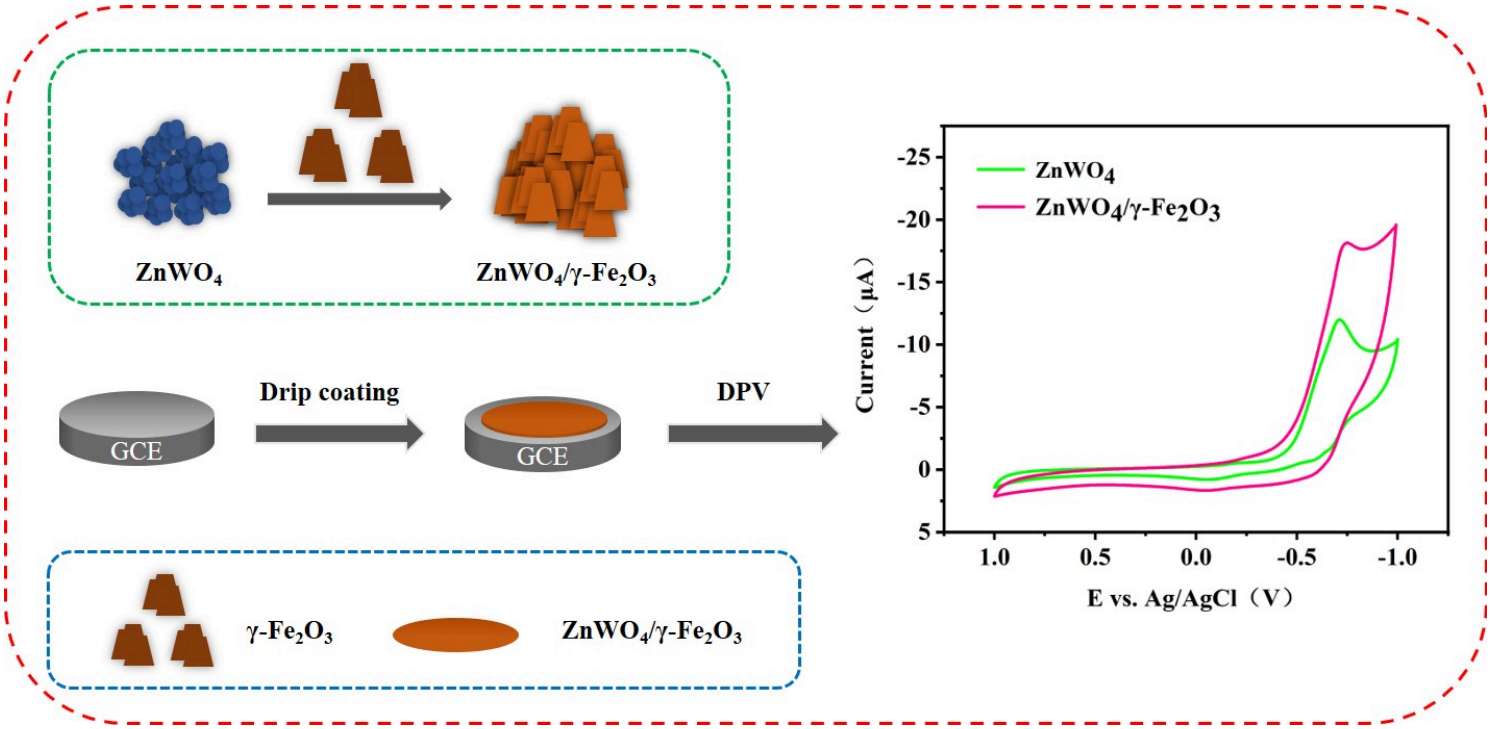


Figure 1

Schematic diagram of synthesized of $ZnWO_4$/γ-Fe_2O_3 and its application in electrochemical detection of CAP, GCE in the figure is glassy carbon electrode.

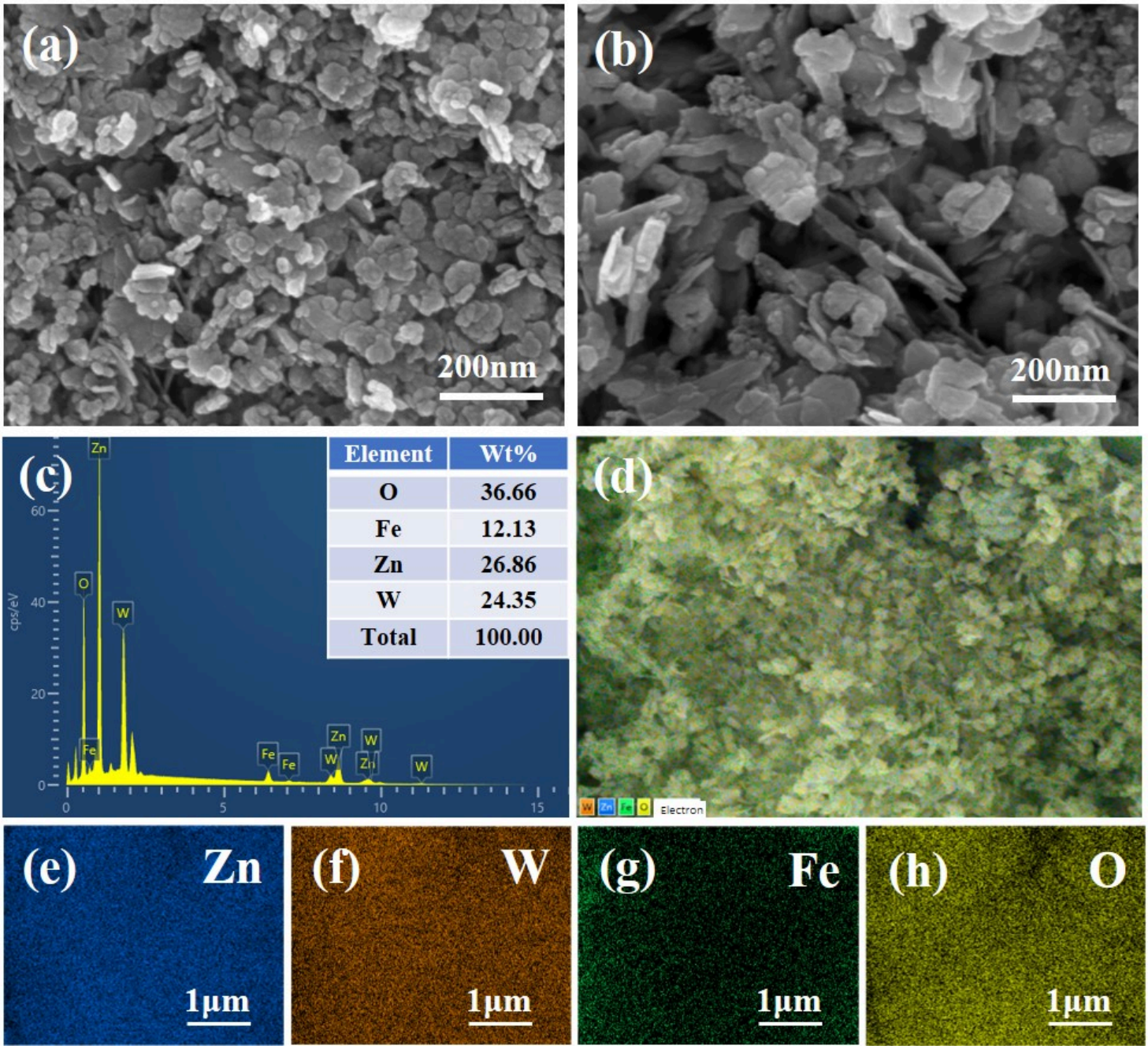


Figure 2

Scanning electron microscope image. (a) SEM image of $ZnWO_4$, (b) SEM image of $ZnWO_4$/γ-Fe_2O_3, (c) SEM-EDS spectra of $ZnWO_4$/γ-Fe_2O_3, (d) prepared $ZnWO_4$/γ-Fe_2O_3 element maps, including (e) Zn, (f) W, (g) Fe and (h) O.

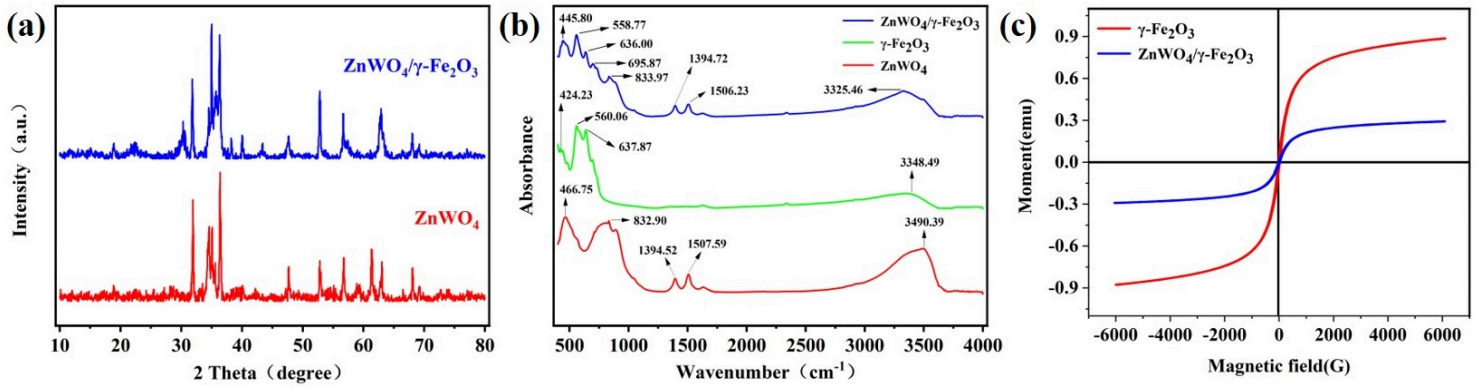


Figure 3

Characterization. (a) XRD pattern; (b) FT-IR spectrum; (c) VSM.

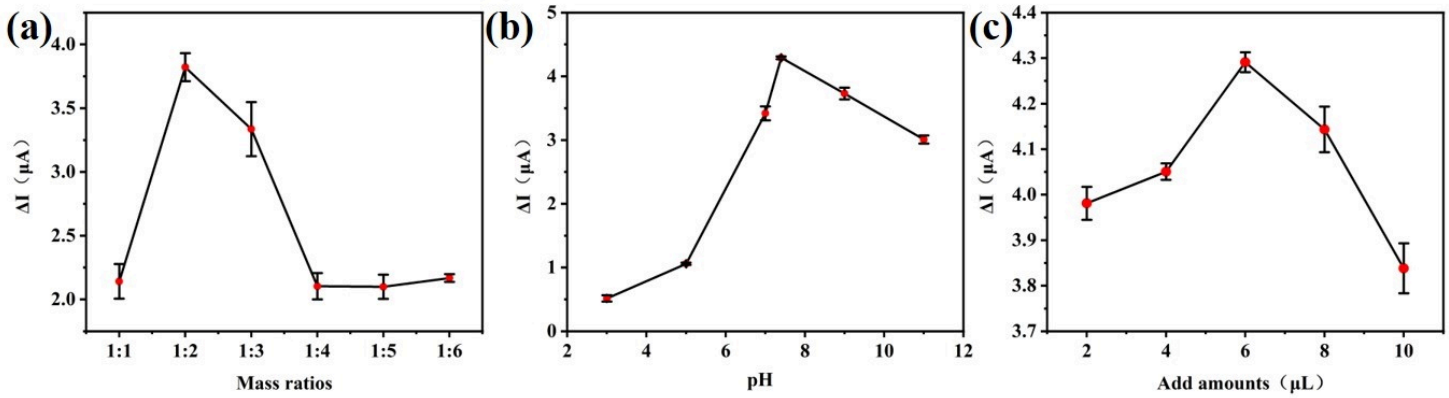


Figure 4

Optimization of experimental parameters. (a) mass ratio of γ-Fe_2O_3 to $ZnWO_4$; (b) PBS solution pH; (c) $ZnWO_4$/γ-Fe_2O_3/MIP load.

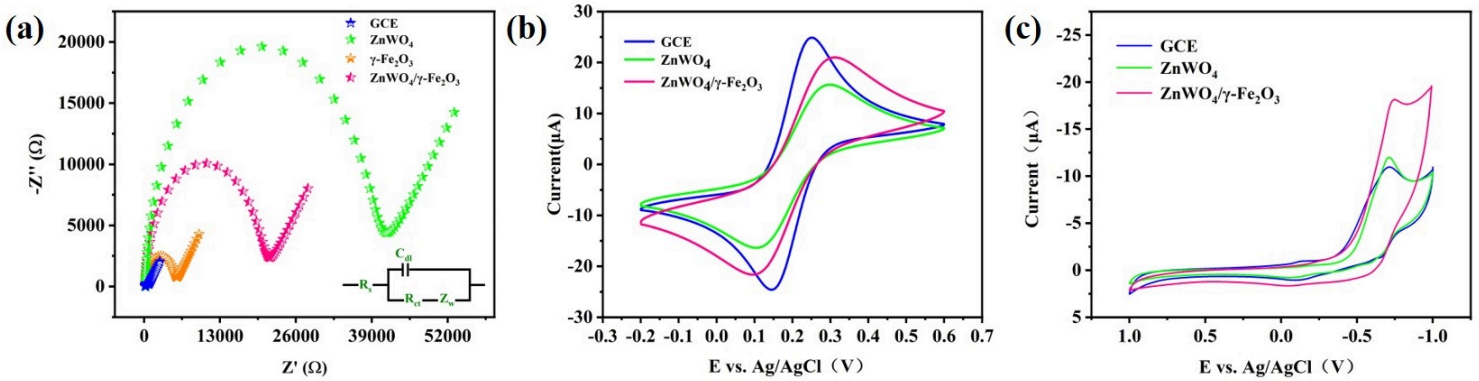


Figure 5

Electrochemical characterization. (a) Impedance curves of various electrodes in 0.1 M KCl and 5.0 mM $[Fe(CN)_6]^{3-/4-}$ solutions; (b) CV curves of various electrodes in 0.1 M KCl and 5.0 mM $[Fe(CN)_6]^{3-/4-}$ solution (scan rate: 50 mV s^{-1}); (c) CV curves of naked GCE, $ZnWO_4$/GCE, $ZnWO_4$/γ-Fe_2O_3/GCE in the presence of 250 μM CAP (solution: 0.01 M PBS (pH = 7.4), scan rate: 50 mV s^{-1}.

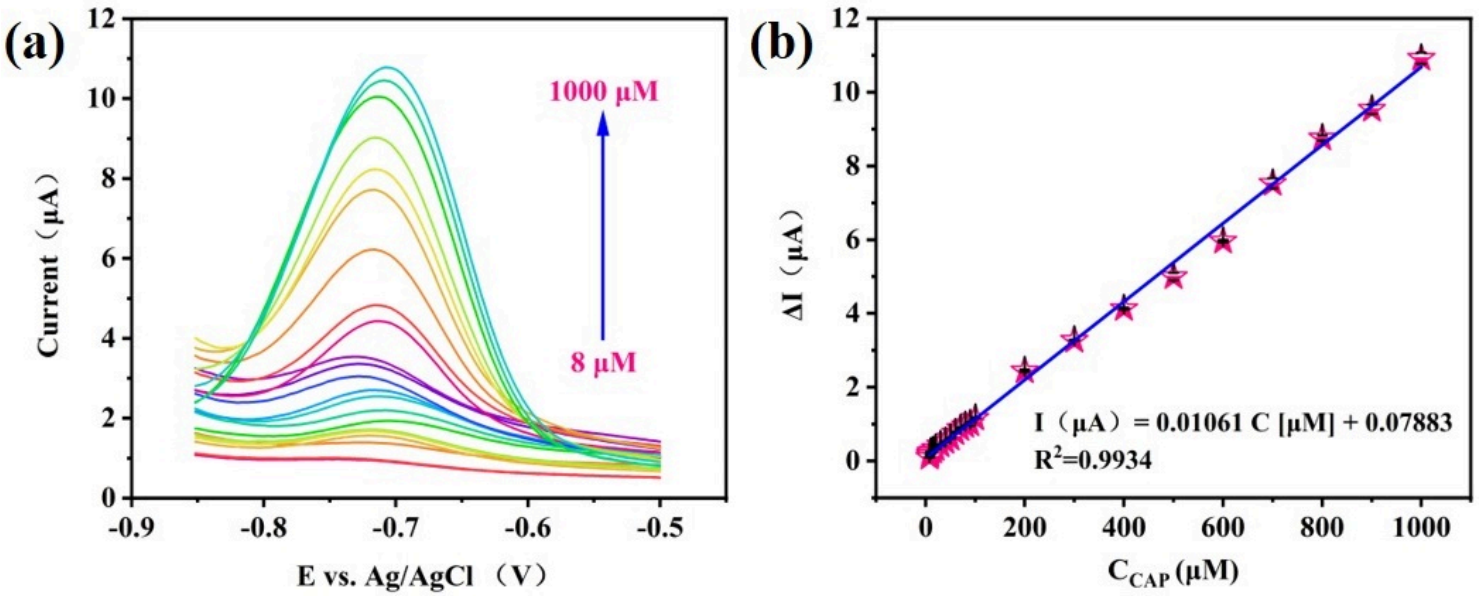


Figure 6

Electrochemical measurements. (a) DPV curves of $ZnWO_4$/γ-Fe_2O_3/GCE in 0.01 M PBS (pH = 7.4) with different CAP concentrations (8~1000 μM); (b) Linear fit of peak current corresponding to CAP concentration

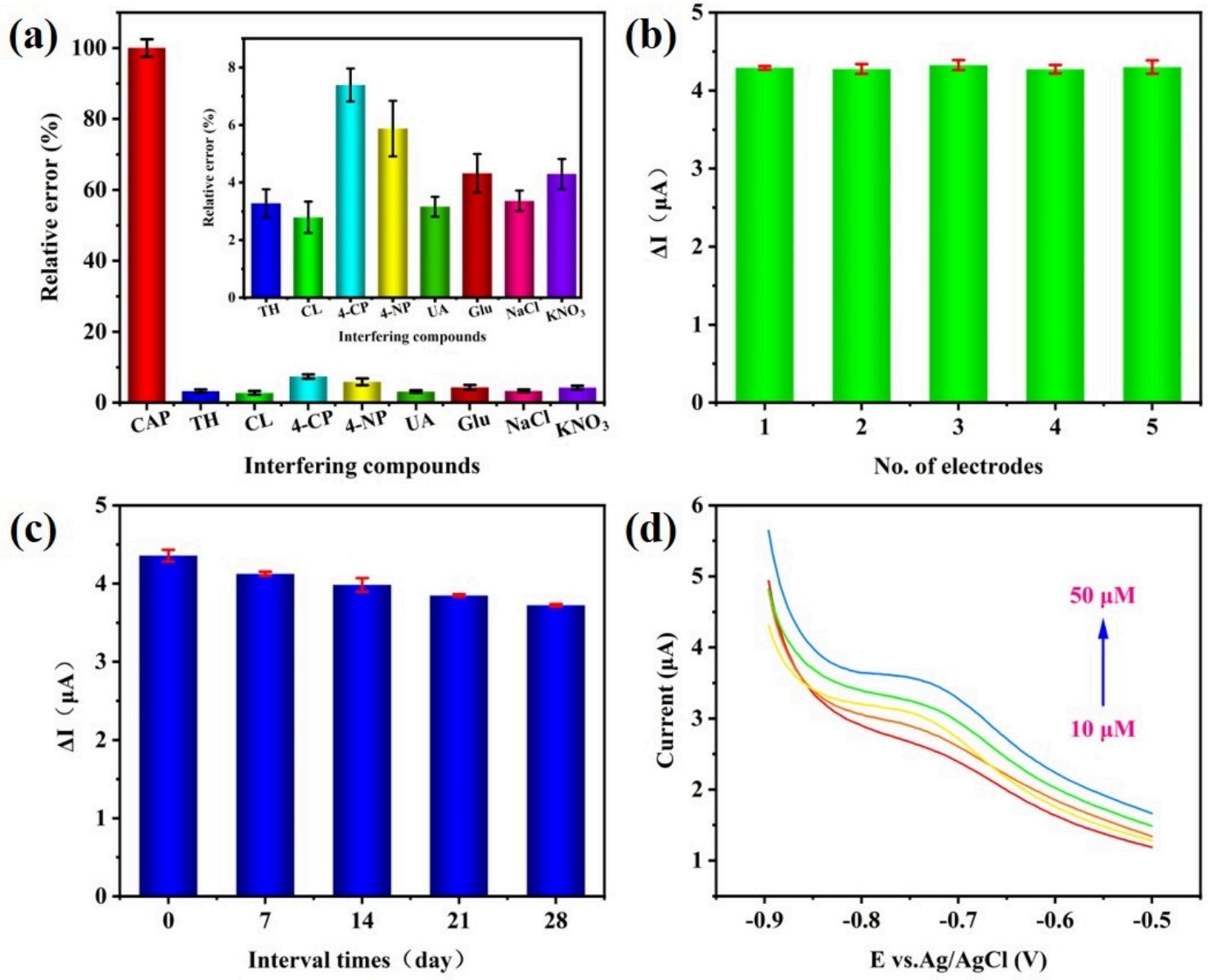


Figure 7

(a) Bar plot of relative error and interfering substances, (b) $ZnWO_4$/γ-Fe_2O_3 modifies the current response of different GCEs to CAP, (c) the current response of $ZnWO_4$/γ-Fe_2O_3/GCE to CAP varies with storage time; (d) DPV responses of the CAP in milk. All experiments were performed with 250 μM CAP in 0.01 M PBS (pH = 7.4)